AIP | The Journal of Chemical Physics

Diffusion and spectroscopy of water and lipids in fully hydrated dimyristoylphosphatidylcholine bilayer membranes

J. Yang, C. Calero, and J. Martí

Citation: The Journal of Chemical Physics **140**, 104901 (2014); doi: 10.1063/1.4867385
View online: http://dx.doi.org/10.1063/1.4867385
View Table of Contents: http://scitation.aip.org/content/aip/journal/jcp/140/10?ver=pdfcov
Published by the AIP Publishing

THE JOURNAL OF CHEMICAL PHYSICS **140**, 104901 (2014)

Diffusion and spectroscopy of water and lipids in fully hydrated dimyristoylphosphatidylcholine bilayer membranes

J. Yang,[1] C. Calero,[1,2] and J. Martí[1,a)]
[1]*Department of Physics and Nuclear Engineering, Technical University of Catalonia-Barcelona Tech, B4-B5 Northern Campus, Jordi Girona 1-3, 08034 Barcelona, Catalonia, Spain*
[2]*Center for Polymer Studies, Department of Physics, Boston University, 590 Commonwealth Avenue, Boston, Massachusetts 02215, USA*

(Received 13 September 2013; accepted 19 February 2014; published online 10 March 2014)

Microscopic structure and dynamics of water and lipids in a fully hydrated dimyristoylphosphatidylcholine phospholipid lipid bilayer membrane in the liquid-crystalline phase have been analyzed with all-atom molecular dynamics simulations based on the recently parameterized CHARMM36 force field. The diffusive dynamics of the membrane lipids and of its hydration water, their reorientational motions as well as their corresponding spectral densities, related to the absorption of radiation, have been considered for the first time using the present force field. In addition, structural properties such as density and pressure profiles, a deuterium-order parameter, surface tension, and the extent of water penetration in the membrane have been analyzed. Molecular self-diffusion, reorientational motions, and spectral densities of atomic species reveal a variety of time scales playing a role in membrane dynamics. The mechanisms of lipid motion strongly depend on the time scale considered, from fast ballistic translation at the scale of picoseconds (effective diffusion coefficients of the order of 10^{-5} cm^2/s) to diffusive flow of a few lipids forming nanodomains at the scale of hundreds of nanoseconds (diffusion coefficients of the order of 10^{-8} cm^2/s). In the intermediate regime of subdiffusion, collisions with nearest neighbors prevent the lipids to achieve full diffusion. Lipid reorientations along selected directions agree well with reported nuclear magnetic resonance data and indicate two different time scales, one about 1 ns and a second one in the range of 2–8 ns. We associated the two time scales of reorientational motions with angular distributions of selected vectors. Calculated spectral densities corresponding to lipid and water reveal an overall good qualitative agreement with Fourier transform infrared spectroscopy experiments. Our simulations indicate a blue-shift of the low frequency spectral bands of hydration water as a result of its interaction with lipids. We have thoroughly analyzed the physical meaning of all spectral features from lipid atomic sites and correlated them with experimental data. Our findings include a "wagging of the tails" frequency around 30 cm^{-1}, which essentially corresponds to motions of the tail-group along the instantaneous plane formed by the two lipid tails, i.e., in-plane oscillations are clearly of bigger importance than those along the normal-to-the plane direction. © *2014 AIP Publishing LLC*. [http://dx.doi.org/10.1063/1.4867385]

I. INTRODUCTION

Biological membranes are ubiquitous in nature as limiting structures of cells, separating cell contents from external environments, but allowing the passage of nutrients and wastes through them. Phospholipid membranes provide the framework to biological membranes, to which other molecules (such as proteins or cholesterol) attach. They consist of two leaflets of amphiphilic lipids which self-assemble due to the hydrophobic effect.[1] The study of pure component membranes can help understand basic biological membrane functions and its interaction with the environment. Among a wide variety of lipids, dimyristoylphosphatidylcholine (DMPC) are phospholipids incorporating a choline as a head-group and a tail-group formed by two myristoyl chains. They are usually synthesized to be used for research purposes (studies of liposomes and bilayer membranes). Their properties are very similar to those of dipalmitoylphosphatidylcholine (DPPC) which has the same structure but slightly longer tails, being a major constituent of pulmonary surfactants of lungs[2] (about 40%).

Structure and dynamics of lipid bilayers in water environments have been thoroughly analyzed from long time ago from the experimental and theoretical points of view, including water permeation and lipid hydration.[3–5] Structure and dynamics have been well characterized by Fourier transform infrared spectroscopy (FTIR) and from quasi-elastic neutron scattering (QENS), whereas hydration of lipid membranes can be probed by means of ultrafast polarization selective vibrational pump-probe spectroscopy,[6] among a variety of techniques. Nevertheless, its microscopic dynamics remains controversial due to the multiple time scales involved (see for instance Ref. 7). Indeed, while at short timescales the dynamics of lipids is dominated by fast translations restricted by their neighbors (*rattling in a cage* effect), at long timescales

a)Author to whom correspondence should be addressed. Electronic mail: jordi.marti@upc.edu

the motion of lipids exhibits a slower long-range diffusion. To reconcile both regimes, a mechanism based on the hopping of lipids to nearby spontaneously created voids was proposed. This paradigm offered an explanation to the apparent contradiction of the lipid motion at different timescales and was instrumental to interpret QENS backscattering experiments.[8] However, this mechanism was recently challenged by different computational[9] and experimental studies,[10,11] in which it is found that the dynamics of lipids at long timescales is collective in nature, strongly correlated over tens of nanometers to the dynamics of the neighboring lipids. This concerted motion creates lipid flow patterns at the mesoscopic scale. In addition, lipid dynamics can be affected by rare event phenomena such as lipid flip-flops (translocations of a lipid chain between the two leaflets composing a membrane), occurring at a time scale of the order of hundreds of nanoseconds[12] and for that reason requiring specific computational tools to analyze them, such as transition path sampling.[13]

Spectroscopic methods provide a valuable tool to help uncover the mechanisms of lipid dynamics. Together with FTIR and QENS mentioned above, other techniques such as small angle scattering of synchrotron radiation, dielectric spectroscopy, and nuclear magnetic resonance have also provided valuable information on the properties of lipid bilayers.[14,15] However, experimental data are often not conclusive and it requires theoretical interpretation. In that respect, molecular dynamics simulations of lipid bilayers can be used to ascertain the microscopic mechanisms responsible for experimental observations. In that spirit, we report in the present work a detailed study of the structure and dynamics of DMPC lipid bilayers. Similar works have been already published using other force fields[14,16,17] but, up to our knowledge, this is the first article where results of dynamical properties such as long time diffusion and spectroscopy have been obtained with the present potential model (CHARMM36[18]). In particular, we focused our view on three particular issues: (1) the characterization of the structure and dynamics of DMPC, (2) the analysis of the microscopic mechanisms of diffusion at different timescales, and (3) the characterization of the motion of atoms (water and lipids) by calculating spectral densities, which can be related to a variety of spectroscopic experimental techniques.

We provide the details of the simulations in Sec. II and explain the main results of the work in Sec. III, focusing our attention especially on the mechanisms of lipid diffusion (Sec. III D), on reorientational motions, and also on the vibrational motions of lipid atoms, described in Sec. III E. Finally, some concluding remarks are outlined in Sec. IV.

II. COMPUTATIONAL DETAILS

Our system is a prototype model of an aqueous bilayer membrane composed by 128 lipids distributed in two leaflets of 64 flexible DMPC molecules surrounded by 4377 TIP3P water molecules. In contrast to the original TIP3P force field,[19] the water model employed in this work allows flexible internal motions (bending, stretching) of water molecules, in order to compute specific spectral densities (see Sec. III E). The main characteristics of the flexible TIP3P water model

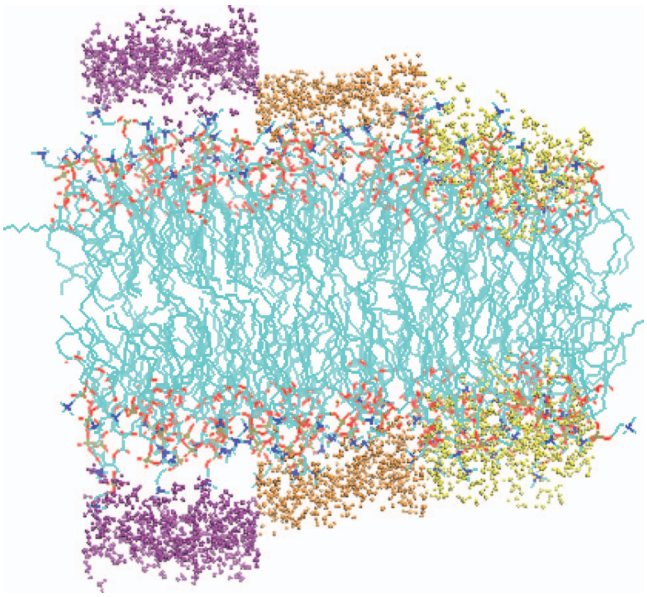

FIG. 1. Snapshot of the DMPC bilayer membrane simulated in this work. The carbon chains of DMPC molecules are shown in cyan. Nitrogen atoms are depicted in blue, phosphorus in green, and ester oxygens in red. Water molecules have been represented in different colors depending on their location: in purple those located at 6 Å or more from any site of a lipid chain ("bulk"); in orange those located between 6 and 3 Å from any lipid site ("intermediate"), and in yellow those located closer than 3 Å of any lipid site ("contact").

were published by Praprotnik and Janežič:[20] average molecular OH bond length of 0.9572 Å and a molecular bond angle of 104.52°. In the present work, the corresponding values have been 0.976 Å and 100.1°. With ∼34.2 water molecules per lipid, our simulated lipid bilayer can be considered fully hydrated.[21] A general view of the system is represented in Fig. 1. Each DMPC molecule is described with atomic resolution (118 sites). Some of the most relevant sites considered in this work, which will be referred to in the analysis of the results, are highlighted in Fig. 2.

Molecular dynamics simulations were performed by means of the NAMD2 molecular dynamics simulation package[22] at a temperature of 303 K and an average pressure of 1 atm. The simulation time step was set to 2 fs for a long 200 ns run and to 0.5 fs for additional short runs, used to analyze vibrations of hydrogens. The recently parameterized force field CHARMM36, which is able to reproduce the area per lipid in excellent agreement with experimental data, has been used. For the long 200 ns run, all molecular bonds have been left nonrigid, except the bonds made with hydrogens. For the short runs, fluctuations of bond distances and angles associated with hydrogens have been allowed as well. Van der Waals interactions were cut off at 12 Å with a smooth switching function starting at 10 Å. Long ranged electrostatic forces were computed with the help of the particle mesh Ewald method,[23] with a grid space of about 1 Å. Electrostatic interactions were updated every 2 fs. Periodic boundary conditions were applied in all three dimensions. After energy minimization, the system was equilibrated in the NPT ensemble at 1 atm for 30 ns. During the NPT simulation run (constant number of particles, constant pressure and constant temperature) we monitored the surface area per lipid

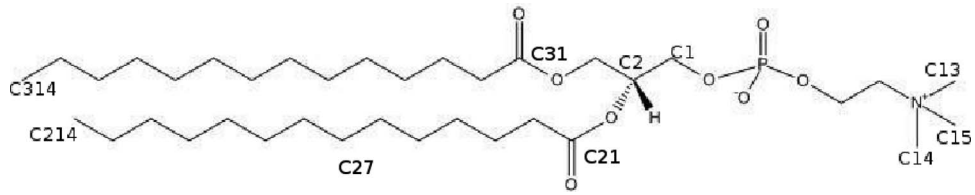

FIG. 2. DMPC molecule with highlighted sites considered in this work. Hydrogen atoms are not shown.

considering the total surface along the *XY* plane (plane parallel to the bilayer surface) divided by the number of lipids in one lamellar layer.[24] The final area per lipid was 60.5 Å^2 (see the top panel of Fig. 3), which is consistent with the expected result of CHARMM36 force field (60.8 Å^2)[18] and also with the experimental value (60.6 Å^2).[25] The reader should note that this value for the area per lipid arises naturally from the relaxation of the system at a given temperature, pressure, and number of particles rather than being an imposition to fit the experimental value. Its agreement with the experimental value validates both the use of the CHARMM36 force field and the chosen equilibration procedure.

Next, a 200 ns production run was performed in the NVT ensemble (constant number of particles, constant volume and constant temperature), with *XY* plane fixed at 67.4 Å × 57.4 Å, which was the final size of the previous equilibrating NPT simulation, and *Z* direction (normal to the *XY* plane) fixed at 140 Å. The temperature was controlled by a Langevin thermostat[26] with a damping coefficient of 1 ps^{-1} for both NPT and NVT simulations, whereas the pressure was controlled by a Nosé-Hoover Langevin barostat[27] with a piston oscillation time of 200 fs and a damping time of 100 fs for the NPT simulation. Since one important goal of this work is to characterize the diffusion of water and lipids over several time scales, we conducted simulation runs of different lengths with appropriately chosen data recording frequencies (see Table I). Finally, in order to eliminate any artificial drift of the center-of-mass (CoM) of the system in the simulations, the coordinates of lipid atoms were corrected for the motion of the center-of-mass of the monolayer to which they belong.[28]

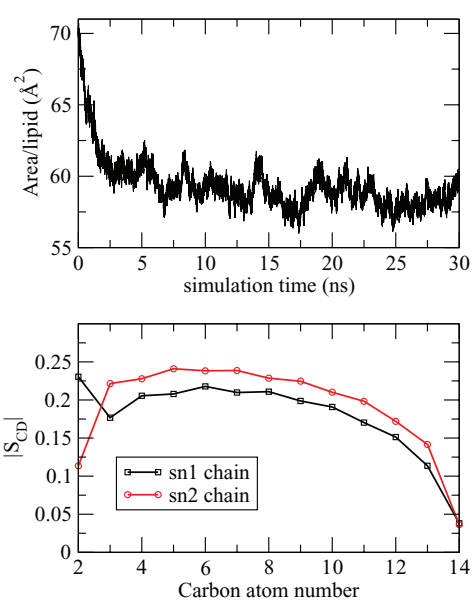

FIG. 3. Area per lipid as a function of simulation time (top) and order parameter for selected carbon sites at the tail-groups (bottom).

To ensure that we are simulating the liquid phase of the model system as well as to efficiently characterize the order of the hydrated lipid bilayer, we computed the deuterium order parameter S_{CD} which can be obtained from ^{2}H NMR experiments. This quantity was first reported by Stockton and Smith[29] and later on adapted by Hofsäss *et al.*,[30] by means of an order parameter defined for each CH_2 group as follows:

$$S_{CD} = \frac{1}{2}(3\langle\cos^2\theta_{CD}\rangle - 1), \tag{1}$$

where θ_{CD} is the angle between the membrane normal and a CH-bond (a CD-bond in the experiments). Brackets in Eq. (1) indicate ensemble average for all lipids. The results are shown in the bottom panel of Fig. 3 for the two chains (sn1, sn2) of a DMPC molecule. The results are in good agreement with both experimental[31,32] and simulation works[5,30,33,34] and confirm that the system, in the simulation conditions assumed in the present work, pertains to the liquid phase.

III. RESULTS

A. Pressure profile and surface tension of the membrane

The pressure profile, i.e., lateral minus normal pressure as a function of the *Z* coordinate, has been obtained from a series of 10 additional simulations (total run length of 20 ns) in the NPT ensemble, in order to better control pressure fluctuations of the system, which strongly affect the pressure at the membrane. Along such short runs, the *XY* dimensions were fixed at 67.4 Å × 57.4 Å while the box *Z* coordinate (fluctuating around 70 Å) was allowed to adjust to the pressure of 1 atm. The remaining parameters were kept the same as those employed during the equilibration run.

The result is displayed in Fig. 4. Our results agree qualitatively well with those reported in a previous work,[35] with some differences observed at relevant regions of the

TABLE I. Simulation lengths and frequency of recording data for the study of diffusion of water and dynamics of lipids at the *ballistic, sub-diffusive*, and *diffusive* regimes.

Purpose	Length	Frequency
Ballistic	10 ps	1 fs
Sub-diffusive	1 ns	100 fs
Fickian (longtime)	200 ns	10 ps
Water diffusion	50 ps	5 fs

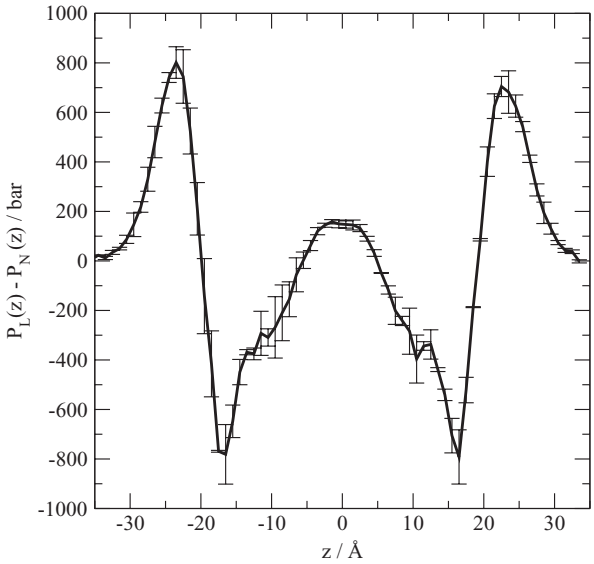

FIG. 4. Pressure profile: $P_L(z) - P_N(z)$.

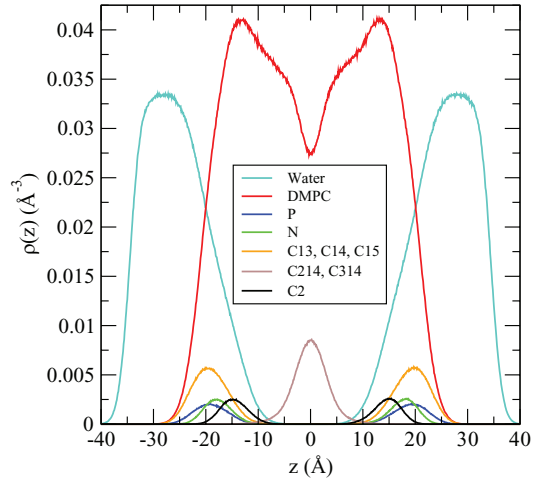

FIG. 5. Density profiles of water, lipid chains, and lipid atoms. Nitrogen (N), phosphorus (P), carbons: C2 (close to the center of mass of the lipid), C13, C14, and C15 (head-group), and C214 and C314 (tail-group).

membrane, i.e., the water-lipid interface and the center of the membrane where the two leaflets are in close contact through tail-tail interactions. We observe significant fluctuations alongside the bilayer of the same order of magnitude already found in previous simulation works.[35] The uncertainty of the pressure profile, represented in the error bars of Fig. 4, was estimated by calculating the absolute difference of the results obtained from each of the ten independent simulations and their average. From the pressure profile we calculated the surface tension γ using,[36] i.e.,

$$\gamma = \int_{-\frac{h}{2}}^{\frac{h}{2}} \mathrm{d}z\,[P_N - P_L]\,, \tag{2}$$

where h is the height of the simulated system's volume, with the normal and lateral pressures given by $P_N = P_{zz}$ and $P_L = \frac{1}{2}(P_{xx} + P_{yy})$, respectively. Here, P_{ii} with $i = x, y, z$ are components of the stress tensor for a bilayer whose normal is parallel to the Z-axis. From Eq. (2), we obtain for the surface tension $\gamma = -0.1 \pm 1.2$ mN/m, again in good agreement with previous works[37] (gel phase, low hydration)[35] (liquid phase). From experimental and theoretical previous works, the expected surface tension of a lipid bilayer membrane should be zero.[37–41]

B. Structure

The local structure of the system can be resolved by means of atomic density profiles, shown in Fig. 5. We sliced the system into 0.1 Å width layers perpendicular to the Z-axis. The overall results are in accordance with those of Griepernau and Böckmann,[34] who employed a different force field in the description of the lipids.

We have considered the densities of nitrogen, phosphorus, and carbon atoms close to the center of mass of the lipids, carbons at the head and tails of lipids, water, and the lipid backbone (excluding hydrogens). A closer look into water densities allows us to distinguish the three regions sketched in the snapshot of Fig. 1: Region (a) "bulk" water (more than 6 Å away from the position of any lipid site), (b) "intermediate" water (between 3 and 6 Å of any lipid site), and (c) "contact" (interfacial) water (within 3 Å of any lipid site). From a general perspective, the structure of the lipid bilayer shows few differences compared to the one obtained by means of the previous CHARMM27 force field.[17]

To investigate the distribution of water molecules around lipid species, we also report selected water-lipid radial distribution functions in Fig. 6. Our results are in good agreement with those recently reported by Hansen *et al.*[17] and indicate a selective binding of water around atoms such as nitrogen and phosphorus and a weak affinity for intermediate carbons as C2, located very close to the center of mass of a lipid chain. As a general fact, water shows a tendency to place around phosphorus at shorter distances (3.8 Å) than around nitrogen (4.3 Å). Further, a second water layer around P can be observed at ∼6 Å, whereas no second layer around N has been detected.

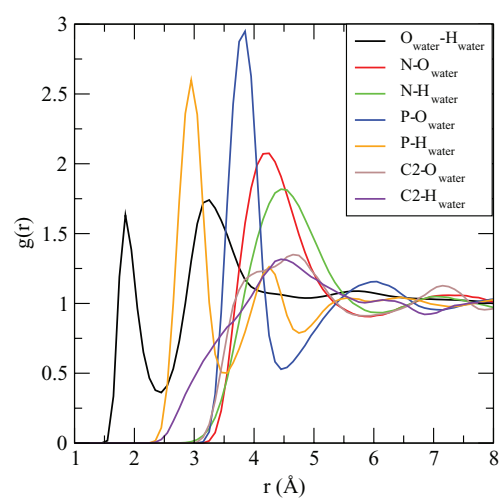

FIG. 6. Radial distribution functions of water (Oxygens, Ow and Hydrogens, Hw) related to several species: nitrogen (N), phosphorus (P), and carbon (C2).

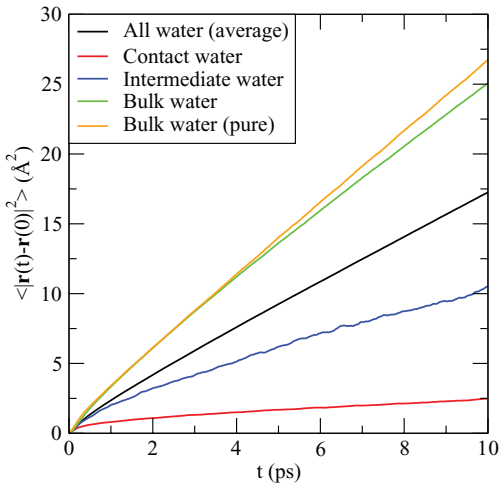

FIG. 7. MSD of water oxygens. The result from the bulk of pure TIP3P water employed in the present work has been included for the sake of comparison with our system's bulk.

C. Water diffusion

Water dynamics in phospholipid membranes has been from long time a controversial issue, with different approaches referring water hydration and its behavior in the vicinity and inside the membrane.[42–44] Water self-diffusion coefficients D_w have been obtained from the analysis of the time-dependence of the mean square displacement (MSD) of oxygen molecules, displayed in Fig. 7. The calculation of D_w renders an overall value of 2.66×10^{-5} cm^2/s, obtained from all water molecules independently of their positions in the system. This can be compared with the self-diffusion of water in a pure system, simulated with the same force field employed in the present work. To do so, we conducted a 50 ps simulation run (after equilibration) in the NVT ensemble. The value of D_w^{pure} has been of 4.0×10^{-5} cm^2/s, indicating that the TIP3P model employed in this work tends to overemphasize water's diffusion. Similar results were obtained by Rosso and Gould.[5]

We have also considered the diffusion of water located in the three different regions defined above: bulk, intermediate, and contact regions. The diffusion coefficient obtained for water in the "contact" region is 0.26×10^{-5} cm^2/s, much smaller than the values obtained for the "intermediate" (1.29×10^{-5} cm^2/s) and "bulk" (3.77×10^{-5} cm^2/s) regions. The latter value is in excellent agreement with the value reported above for pure water, which validates the choice of the "bulk" like region considered in the present work. So, although the water model employed in this work considerably overestimates water diffusion in bulk (the experimental value for the water diffusion coefficient is 2.3×10^{-5} cm^2/s[45]), the drastic drop in water diffusion at the interface should be model independent and related to the interaction of water molecules with the hydrophilic lipid heads.

During the calculation time-window of 10 ps, about ~24% of water molecules remained in the "bulk" group, ~6% water molecules stayed in the "contact" zone, while only ~0.5% of them were accounted as "intermediate" water molecules, with the remaining water molecules fluctuating between different zones. For this reason, statistics at the intermediate zone are much worse than those from the other two regions, which is reflected in the noise observed in the MSD of "intermediate water" reported in Fig. 7.

D. Mechanisms of lipid diffusion

One of the most relevant issues in the study of phospholipid membranes concerns the lateral diffusion of lipid chains. Different factors such as temperature, pressure, amount of cholesterol and proteins, hydration, concentration of salts, etc., may have strong influence on lipid dynamics. Further, a variety of experimental methods report significantly different values for the diffusion coefficient. Experimental studies using pulsed field gradient nuclear magnetic resonance,[46] single particle tracking,[47] fluorescence recovery after photobleaching,[48] or from fluorescence correlation spectroscopy[49] report values within 0.5×10^{-7} cm^2/s and 1×10^{-7} cm^2/s. Neutron scattering experiments, operating in the picosecond range, produce diffusion coefficients significantly higher,[7,8,50] in the range of 1 to 10×10^{-7} cm^2/s.

Furthermore, there exists a controversy concerning the existence of two regimes working on the dynamics of lipids, namely (1) the fast confined motion limited by the neighboring lipids, i.e., *rattling in a cage* effect,[14] probably due to the wagging of lipid tails, as it has been observed for some fatty acids[51] at short timescales and (2) the slower long-range diffusion exhibited at longer timescales. The accepted paradigm is based on a mechanism of lipid hopping out of the neighbor cage to nearby spontaneously created voids, which successfully accounts for QENS backscattering experiments.[8] Such a mechanism was put in question by Falck *et al.*,[9] who studied the lateral diffusion of lipid membranes with MD simulations. They concluded that the dynamics of lipids at long timescales is collective in nature, strongly correlated over tens of nanometers to the dynamics of their neighbors. Later on it was shown that such mechanism was consistent with experiments.[10,11]

Generally, the time-dependence of the lateral MSD of membrane lipids can be described by a power law as follows:

$$\langle \vec{r}^2(t) \rangle \sim A \cdot t^{\beta}, \tag{3}$$

where the exponent β changes for different time scales. At the shortest time scale, lipids undergo ballistic motion (with $\beta \sim 2$), followed by sub-diffusion (with $0 < \beta < 1$) at some intermediate scale, and ending with continuous Brownian motion with $\beta \sim 1$ at the longest time scale available in our computer simulations. We have separated these three time regimes from different parts of MSDs, as illustrated in Fig. 8. The results of β computed for selected lipid atoms (N, P, C15, C2, C at tail's ends) at different time scales are reported in Table II. The results corroborate the choice and denomination of the three relevant time scales.

To characterize the dynamics of lipids at the different time-scales we have computed lateral diffusion coefficients D_L of selected lipid atoms (N, P, C15, C2, and C at tail's ends),

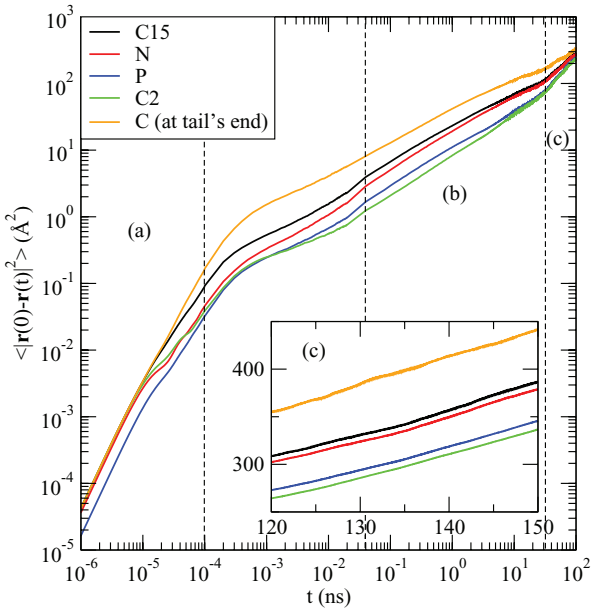

FIG. 8. MSD of lipid atoms. (a) Sub-picosecond time scale; (b) nanosecond time scale; (c) hundred nanoseconds time scale. The inset shows the range of longest time, between 120 and 150 ns.

given by

$$D_L = \lim_{t\to\infty} \frac{\langle|\vec{r}_i(t) - \vec{r}_i(0)|^2\rangle}{4t}. \tag{4}$$

Full results of diffusion coefficients of lipids are reported in Table III, where we have separated results corresponding to the three time scales indicated above, obtained from different parts of the time-dependence of the MSDs of selected lipid sites. We refer to them as *diffusion* coefficients, although real diffusion is only achieved at the longest time scale and in the two shorter time scales we can only compute *effective* diffusion coefficients, which will provide valuable information on the rapidity of atomic motions.

In the sub-picosecond time scale (between 1 fs and 0.1 ps, Fig. 8(a)) β ranges between 1.92 and 1.96, indicative of ballistic motion (see Table II). In that regime we observe fast motion of all atoms in the lipids, with effective diffusion coefficients of the order of 10^{-5} cm^2/s (see Table III). This is an indication of flow-like ballistic diffusion, with all atoms acting as free inertial particles. We note that atoms belonging to the same lipid can move up to 2.5 times faster than others, e.g., tail carbons (C214 and C314) compared to phosphorus.

TABLE II. Exponent β of lipid atoms corresponds to *ballistic motion*, *sub-diffusion*, and *long time (Fickian) diffusion*.

Atom	$\beta_{ballistic}$	$\beta_{sub-diffusive}$	$\beta_{Fickian}$
N	1.94	0.57	1.04
P	1.96	0.62	1.08
C15	1.94	0.54	1.04
C2	1.92	0.62	1.11
C (at tail's end)	1.94	0.49	0.90

TABLE III. Effective and real diffusion coefficients of atomic species in lipids (in 10^{-7} cm^2/s) obtained at different time scales. *Ballistic* corresponds to the 0.1 ps time scale, *sub-diffusive* corresponds to the 0.3 ns time scale, and *Fickian* has been obtained at the 150 ns time scale.

Atom	$D_{ballistic}$	$D_{sub-diffusive}$	$D_{Fickian}$
N	92	4.30	0.65
P	48	2.84	0.61
C15	120	5.05	0.66
C2	105	2.18	0.61
C (at tail's end)	121	8.8	0.65

In between, carbons at lipid heads (C15) tend to move at rates of $\sim 120 \times 10^{-7}$ cm^2/s.

At a longer time scale (range between 0.01 and 10 ns, Fig. 8(b)), the so-called *sub-diffusive* regime,[16] we obtain different values for the effective diffusion coefficient, of the order of $\times 10^{-7}$ cm^2/s. In this regime the MSD scales with $0 < \beta < 1$, see Eq. (3). We obtained values for β between 0.49 for carbons at the final sites of tail-groups and 0.62 for phosphorus or C2. These values are in good agreement with those recently reported by Jeon *et al.*[52] for several different membranes. In this time scale the dynamics is slower due to interactions of the lipid chains with neighboring ones, although they have not reached a pure diffusive regime yet. Our results for the effective diffusion coefficients range between $\sim$2 and 9×10^{-7} cm^2/s. Now the fastest motions are due to carbons located at the lipid tail whereas C2 carbons, close to the center-of-mass of the lipid chain, are the slowest.

Lipid sub-diffusion has been observed in several experiments.[53] The main observation is that MSD can be described by a power law $\langle\vec{r}^2(t)\rangle \sim A \cdot t^\beta$, with a time dependence of MSD in sub-diffusive time scale ($0 < \beta < 1$) weaker than that in Fickian diffusion, where $\beta \sim 1$. However, the physical mechanisms behind sub-diffusion could be diverse according to specific environments. Models such as continuous time random walk, fractional Brownian motion and the fractional Langevin equation (FLE) have been proposed.[54] Based on extensive molecular dynamics simulations, Jeon *et al.*[52] showed that sub-diffusion in lipid bilayers can be described by a FLE-type stochastic motion. We see in our simulations that the length scale explored by lipids in the sub-diffusive regime is comparable and slightly over the typical lipid-lipid distance (see Fig. 8). This suggests that the sub-diffusive regime is reached when a lipid chain crosses a given energy barrier created by the interaction with its nearest neighbors. Lipid bilayer membrane is a crowded environment, where a mobile lipid molecule will be constrained continually by "rattling in a cage" motion due to its local environment. As a result its effective motion is offset, corresponding to a slower MSD increment, i.e., weaker time dependence. After colliding with environments during a given transient time, a lipid chain will move towards a direction where it will have a chance to surmount the energy barrier and escape from its neighbors' cage. The typical time needed for a lipid to find such a comfortable direction, i.e., a place with lower energy barrier is the intermediate time scale with $\beta < 1$ observed before the linear MSD is achieved. This interpretation is in overall agreement with previous ones.[14]

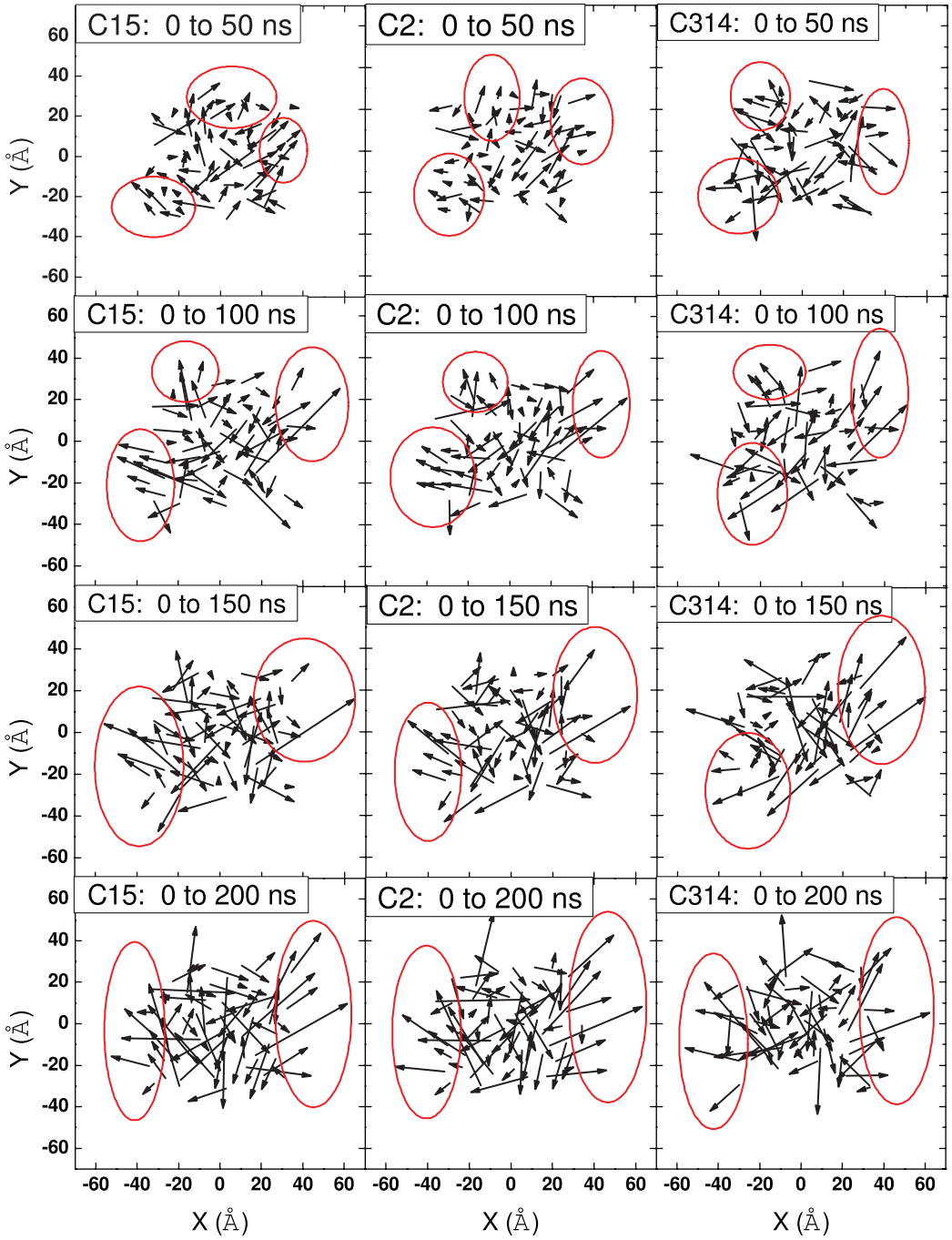

FIG. 9. Contour plots of lipid displacements as a function of time. The displacements are real, i.e., no periodic boundary conditions have been considered. Some nanodomains have been highlighted with red lines.

Finally, full diffusion is practically achieved at the time scale of hundreds of nanoseconds (Fig. 8(c), where $\beta \sim 1$). In that regime the dynamics of lipids is governed by *Fickian* diffusion, i.e., due to gradients of concentration and not mediated by local, short ranged effects as in the case of the previous regimes. Interestingly, at this time scale, all (selected) atoms in the lipid diffuse at approximately the same rate, with diffusion coefficients between 0.61 and 0.66 $\times$ 10^{-7} cm^2/s. This suggests that lateral diffusion of a lipid chain is the result of its global motion. The diffusion coefficient of atom C2, located next to the center-of-mass of the lipid, $D_L = 0.61 \times 10^{-7}$ cm^2/s, is in close agreement with the experimental result obtained from FRAP experiments (at 30 °C) of 0.59 $\times$ 10^{-7} cm^2/s.[55] In contrast, the diffusion coefficient reported from simulations based on the CHARMM27[56] force field by Flenner *et al.*,[16] 1.46 $\times$ 10^{-7} cm^2/s, is in clear discrepancy with the experimental value. Thus, it seems clear that the CHARMM36 force field accounts better than CHARMM27 for the diffusion of DMPC lipids in bilayer membranes.

To further investigate the diffusive dynamics of lipids at long timescales, we have depicted in Fig. 9 the time evolution of the displacements of lipid chains belonging to one single monolayer. The physical features reported here were observed independently for the two lipid monolayers. We tracked three

atoms of each lipid chain (C15, C2, C314, located at the lipid head, center, and tail, respectively) during different instants of the simulated trajectory (50, 100, 150, and 200 ns). As shown in Fig. 9, after 50 ns the displacements of all lipid sites considered are already evident. After 100 ns, longer displacements are seen in all cases, with some indication of the appearance of *nanodomains* or collective local motions, for all classes of particles considered, identified in Fig. 9 with red ellipses. For longer times, the regions where lipid species move in a concerted way are evident for all sites. At times up to 200 ns, the particles keep moving the same way. Within the timescales explored, the direction of the motion of the identified nanodomains seem to be conserved in time, with all three sites (C15, C2, and C314) moving roughly towards the same direction. This is in agreement with the fact that diffusion coefficients are fully equivalent at the Fickian regime (variations smaller than 10%, see Table III).

In summary, we observed that neighboring lipids forming nanodomains move concertedly in a particular direction within the plane of the membrane. This reveals a mechanism of diffusion based on collective flows of a limited number of lipid chains, which results in diffusion coefficients of the order of 0.6×10^{-7} cm^2/s. This conclusion is in overall agreement with the computer simulation's findings of Falck *et al.*[9] and the QENS data of Busch *et al.*,[10] although in our case the size of the lipid clusters formed is smaller, of the order of 10 lipid chains.

E. Spectral densities of water and lipid species

In this section we analyze the spectral densities of water oxygens, water hydrogens, as well as of selected atomic sites at the DMPC molecules. Experimental infrared spectra are usually obtained through the absorption coefficient $\alpha(\omega)$ or the imaginary part of the frequency-dependent dielectric constant.[57] These properties are directly related to the absorption lineshape $I(\omega)$, which can be obtained from molecular dynamics simulations[20,58] in certain cases, as it will be highlighted below.

The spectral density $S(\omega)$ is defined as

$$S_i(\omega) = \int_0^\infty \mathrm{d}t\ C_i(t)\cos(\omega t), \tag{5}$$

where $C_i(t) = \langle \vec{v}_i(t)\vec{v}_i(0)\rangle$ is the velocity autocorrelation function (VACF) for atom i. In our case $i = \mathrm{O}_{water}$, H_{water}, H_{lipid}, N, P, C2, C15, C27, C214, and C314 (average of the latter two), with the brackets $\langle\cdots\rangle$ denoting equilibrium ensemble average.

In the case of water, it has been shown that $S(\omega)$ is directly related to $I(\omega)$, giving

$$\begin{aligned} I(\omega) &= \frac{1}{2\pi}\int_{-\infty}^{\infty} \mathrm{d}t\ \langle \vec{M}(t)\vec{M}(0)\rangle \cos(\omega t) \\ &= \frac{1}{\pi\omega^2}\int_0^{\infty} \mathrm{d}t\ \langle \dot{\vec{M}}(t)\dot{\vec{M}}(0)\rangle \cos(\omega t), \end{aligned} \tag{6}$$

where $\vec{M}(t)$ is the total dipole moment of water.[58] The final expression has been obtained by repeated integration by parts and using time symmetry. For three-site water models with partial charges (such as the TIP3P model), we can write

$$\dot{\vec{M}}(t) = q\sum_{i=1}^{2N}\vec{v}_{H_i}(t) - 2q\sum_{i=1}^{N}\vec{v}_{O_i}(t), \tag{7}$$

where q stands for the effective hydrogen charge, N is the total number of water molecules in the system, and $\vec{v}_{O_i(H_i)}$ is the velocity of the oxygen (hydrogen) of atom i at time t. Using this expression in Eq. (6) we obtain terms with self and cross velocity correlation functions. It has been proven[58] that the terms including oxygen velocities have minor influence in the final result of the absorption lineshape and can be neglected, and Eq. (6) becomes

$$I(\omega) \approx \frac{2Nq^2}{\pi\omega^2} S_{H_{water}}(\omega). \tag{8}$$

From Eq. (8) we see that knowledge of the lineshape $I(\omega)$ can be used to study the motion of water hydrogens. Hence, although classical molecular dynamics simulations are not able to fully reproduce experimental absorption coefficients, these being quantum properties, they can be used to locate the position of the spectral bands since in the harmonic (oscillator) approximation classical and quantum fundamental frequencies are the same.

We characterize the vibration of the center of mass of water by computing its corresponding spectral density $S_{water}(\omega)$, which is displayed in Fig. 10. Such spectral densities are directly related with low frequency bands observed at far infrared and Raman spectroscopy measurements of liquid water.[59,60] The three groups of water molecules defined in Sec. III B have been considered. We observe spectral shifts in good qualitative agreement with results obtained for a DPPC membrane.[61] For bulk water, the two main bands in the range of mid-infrared vibrations (experimentally located at 60 and 170 cm^{-1}[62]) are present, the lowest frequency centered at about 35 cm^{-1} and the highest one at around 225 cm^{-1}. For water molecules located next to lipid atoms (intermediate and contact regions) the first low frequency peak blue-shifts, whereas the highest frequency band remains unchanged. In addition, for water in close contact with lipid sites, the signature of hydrogen-bonding shows a marked tendency to disappear. The first peak is usually related to hindered vibrations of a water molecule in the cage of its nearest neighbors (*rattling* in a cage), whereas the band centered around 200 cm^{-1} is associated with stretching vibrations of hydrogen-bonds.[63] The disappearance of this second peak seems to suggest that water molecules in contact with lipid sites tend to form a lower number of hydrogen-bonds.

The spectral density corresponding to the water's hydrogens, directly related to the absorption lineshape of radiation (see Eq. (8)), is shown in Fig. 11. In the spectra, three regions need to be distinguished: one for frequencies up to 1000 cm^{-1} (librational motions), a second one for frequencies between 1000 and 2000 cm^{-1} (bending motions), and a third spectral band between 2000 and 4000 cm^{-1} (stretching motions). We observe in Fig. 11 that stretching vibrations of water reveal a broad band centered at ≈3360 cm^{-1}, formed by two maxima at 3320 and 3375 cm^{-1}. These results are in good overall agreement with very recent FTIR findings by Disalvo

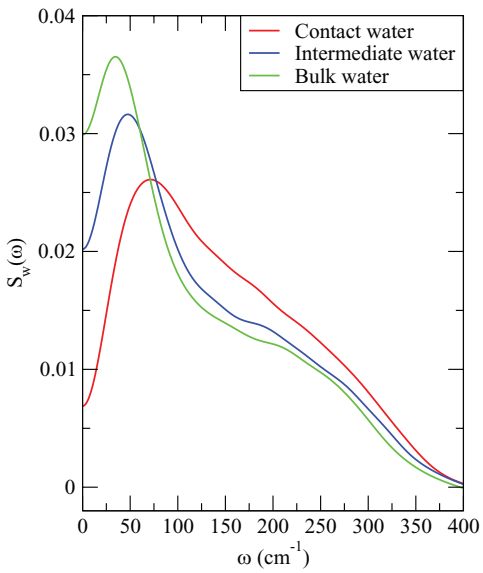

FIG. 10. Spectral densities $S_w(\omega)$ of water's center-of-mass.

and Frias,[64] who observed maxima at 3300 and 3550 cm^{-1} for water in DMPC at 25 °C, what indicates that our second maximum is underestimated by about 175 cm^{-1}. The location of the bending mode is also overestimated, centered around 1795 cm^{-1} in the present work, the experimental value being[64] of 1700 cm^{-1}. Finally, librations are fairly well reproduced, with maxima around 455 cm^{-1}. This agrees well with experimental information available for pure water,[65,66] which indicates the existence of a broad band associated with librations between 300 and 900 cm^{-1}. From the results shown in Fig. 11, we see that hydrogens belonging to water molecules close to lipid chains (contact water) show the same bending and stretching vibrations as bulk water, but at the librational region, associated with molecular rotations, a blue shift of ∼90 cm^{-1} is observed. In contrast, water located between 3 and 6 Å of lipid sites (intermediate) shows the same frequency vibrations as bulk water for all three bands.

Vibrations of hydrogens belonging to lipid chains exhibit significant changes when compared with those of water hydrogens, revealing that molecular motions of hydrogens in lipid chains are significantly slower than those in water: first, the high-frequency stretching band is centered around 3000 cm^{-1} and split into two contributions for hydrogens belonging to lipid heads (2945, 3080 cm^{-1}). This vibration should correspond to CH_3 choline (C–H) stretch vibrations, as we will explain below. This is excellent agreement with findings of Pohle *et al.*[67] and Binder.[68] Second, a very intense band around 1430 cm^{-1} is observed and it should be attributed to the bend of internal CH angles.[68] Further, a band of smaller intensity around 1000 cm^{-1} is also observed and, as we will discuss below, it can be directly attributed to vibrations of carbon units. From the experimental side, Hübner and Mantsch[69] who analyzed phosphatidylcholine multilayers by means of FTIR spectroscopy, attributed this band to vibrations of N-$(CH_3)_3$ units, reported around 970 cm^{-1}. In other experiments, Binder *et al.*[68,70] employed infrared linear dichroism spectroscopy to assign a band around 970 cm^{-1} again to the asymmetrical stretch of CN-$(CH_3)_3$ units. Finally, a libration band is now located around 230–280 cm^{-1}. Remarkably, the values obtained in the present work for lipid hydrogen vibrations are in very good agreement with theoretical data[71] obtained by means of density functional conformational analysis of DMPC membranes.

We have also considered vibrations of other atoms belonging to lipid chains, such as nitrogen, phosphorus, and a variety of carbons. The results are reported in Figs. 12 and 13. As expected, the frequency range for N and P is shorter than that of hydrogens, now ranging from 0 to 1600 cm^{-1}. Three different frequency domains may be defined: (1) at low frequencies, $\omega < 300$ cm^{-1}, restricted translational motions are described; (2) in the range of $400 < \omega < 800$ cm^{-1}, librational motions, including those around dihedral angles as well as slow vibrational modes are involved; (3) for

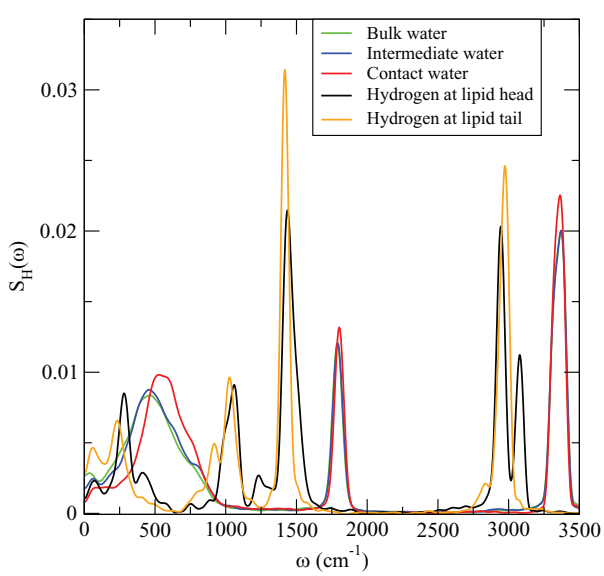

FIG. 11. Hydrogen spectral densities $S_H(\omega)$ for lipid and water species.

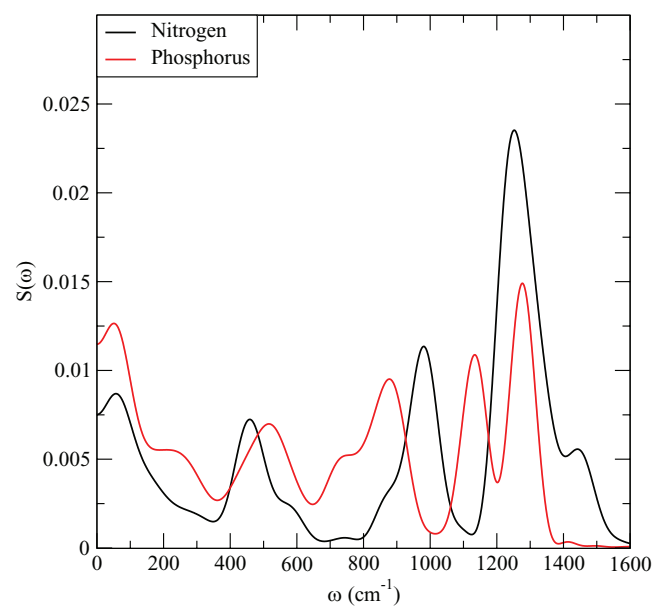

FIG. 12. Spectral densities of nitrogen and phosphorus atoms.

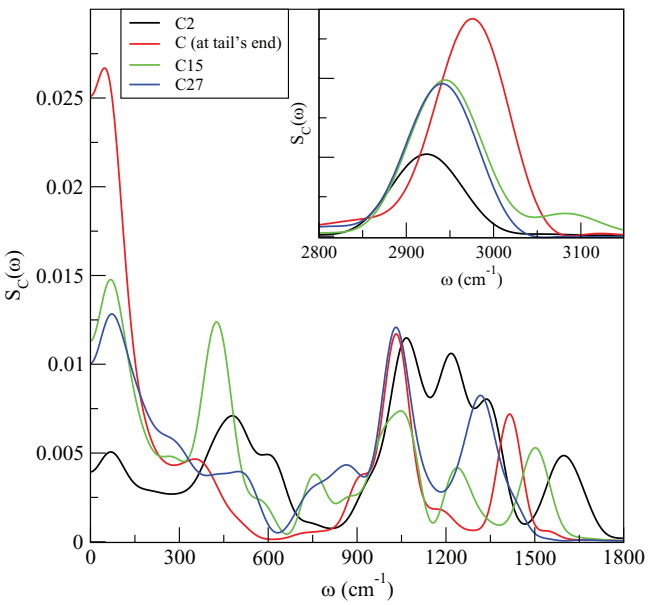

FIG. 13. Carbon spectral densities $S_C(\omega)$. The inset shows the range of highest frequencies, around 3000 cm^{-1}, of small relative intensity.

$800 < \omega < 1600$ cm^{-1}, faster vibrational modes, related to bending and stretching along molecular bonds.

The spectral densities of nitrogen and phosphorus reported in Fig. 12 reveal restricted *rattling-in-a-cage* vibrations for both particles (around 50–60 cm^{-1}) and librational peaks around 460 and 520 cm^{-1}, respectively. This suggests a N-P collective vibrational motion of the full head-group. At higher frequencies, some significant differences arise, indicating that atomic motions of N and P are not directly related. Nitrogen shows a vibration at 980 cm^{-1} that can be associated with the mode obtained around 1000 cm^{-1} for hydrogens (see Fig. 11) and attributed to vibrations of N-$(CH_3)_3$ units (see above). Two additional maxima for N are observed around 1250 and 1450 cm^{-1}. Both should obviously be related to CH_3-N-CH_2 vibrations, since we found evidence of those bands in the C15 spectrum (Fig. 13), but located at 1240 and 1490 cm^{-1}. In the same frequency range, we found a ~875 cm^{-1} frequency peak for P that might be associated with the asymmetric P-$(OC)_2$ stretching motions observed by Binder around 800–830 cm^{-1}.[68,70] At even higher frequencies other two vibrational motions of O–PO_2–O units are seen: one at 1135 cm^{-1} and another one around 1280 cm^{-1}, assigned to the symmetric and asymmetric stretch of O–PO_2–O units,[69,70] respectively. Other authors (Kozak *et al.*[15]) found a single maximum around 1209 cm^{-1}, associated with a PO_2^- stretching mode. The numerical agreement of our data with experimental data of Hübner and Mantsch[69] and with Binder *et al.*[68,70] is quite remarkable.

Finally, spectral densities of carbons are reported in Fig. 13. Four carbon sites at the lipid chains have been selected: C15, C2, C27, and C214 at the head, body center, central part of tails, and tail's end of DMPC, respectively. In this case, four frequency domains can be distinguished: (1) $\omega < 300$ cm^{-1} (restricted translations) all of them in the range of 45–75 cm^{-1}, i.e., slightly higher than those reported for N and P, (2) $300 < \omega < 900$ cm^{-1} (molecular librations), (3) $900 < \omega < 1800$ cm^{-1} (low frequency vibrations of molecular groups), and (4) $2800 < \omega < 3100$ cm^{-1} (high frequency vibrations of molecular groups). In domain (1) the usual hindered translations are seen in all cases; in domain (2) we can observe two prominent peaks around 425 and 490 cm^{-1} for C15 and C2 but no clear vibrations of tail-group carbons are seen. Following this, rotation of lipids may be attributed to librational motions of the head-groups (including C2) in motions which are essentially independent of those performed by tail-groups. Density functional calculations by Krishnamurty *et al.*[71] showed the existence of frequencies in this domain, which were assigned to symmetric deformation modes involving oxygen and carbon units.

In contrast, vibrations in domains (3) and (4) can be related to experimental findings. In the main Fig. 13 we can distinguish two groups of vibrations: one at frequencies around 1000–1200 cm^{-1} and another one for values in between 1315 and 1600 cm^{-1}. For the two cases, all classes of carbons are involved. Vibrations at the lowest frequencies have been related to the motion of phosphorus as well as to the so-called *wagging* motions of CH_2 and CH_3 chains,[67,71,72] whereas at the highest frequencies the bands have been attributed to bending motions of CH_2 groups (located around 1450 cm^{-1}) and to C=O stretching vibrations.[71,72] From our findings, we observe that all spectra considered (including carbon sites not shown, such as C22, C24, C26, C28, C210, and C212) show the two vibrational features, indicating that they can be related to stretch modes along C–C directions (range of highest frequencies) and also bend of C–C–C and C–N–C units. Finally, vibrations around 2950 cm^{-1} assigned to CH_3 choline (C–H) stretch are also observed for carbons and presented in the inset of Fig. 13. There we can observe that carbons at the end of tail-groups show stretching frequencies around 2975 cm^{-1}, i.e., slightly blue-shifted from those of the rest of carbon units. Interestingly, these frequencies have been assigned to vibrations of "head" (CH_3) and "neck" (CH_2) groups,[67,68] assignments which are in excellent qualitative agreement with our present interpretation.

F. Low frequency vibrations of lipid tails and reorientational motions

Among the frequency ranges explored in the present work, perhaps the less known is the one related to low frequency vibrations, up to 100 cm^{-1}, which corresponds to slow motions of parts of the lipid chains. In such range we expect to observe restricted translational motions of few atomic units and also signatures of collective displacements of a group of particles. To further explore the lowest frequency range, we have analyzed the slow motions of lipid tails, and computed reorientational correlation functions and their corresponding characteristic decay times.

A detailed analysis of lipid tail-group motions has been performed through the calculation of velocity autocorrelation functions of the center-of-mass of each tail $\vec{v}_{CoM}$ (labeled "total" in Fig. 14). To provide further insight into the librational motion of the lipid tails, we decomposed $\vec{v}_{CoM}$ into its parallel (called "in-plane") and perpendicular (called "normal")

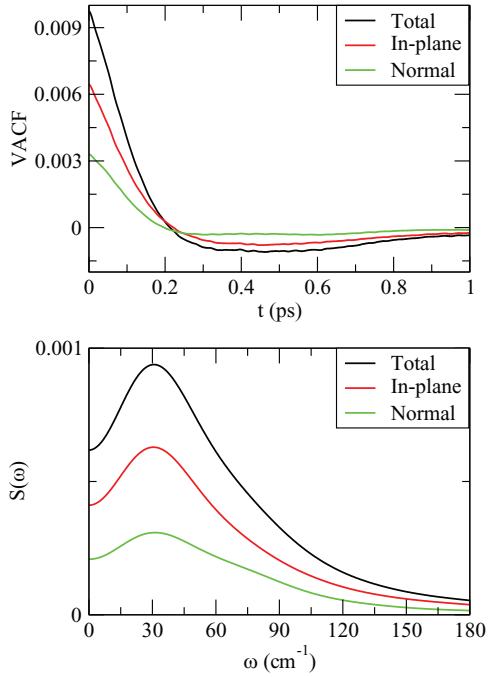

FIG. 14. Velocity autocorrelation functions of single tail's center-of-mass and their spectral densities. The velocities of the CoM of lipid tails (black lines) have been projected on (1) the instantaneous plane formed by the two lipid tails (red line) and (2) the direction normal to the instantaneous plane indicated above (green line).

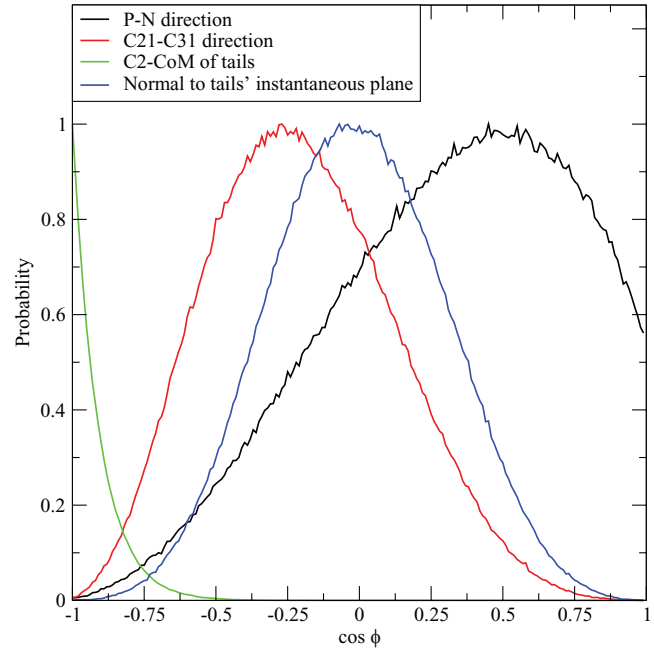

FIG. 15. Angular distributions of unit vectors **u** along selected directions. ϕ are the angles formed by **u** and the Z-axis. P-N direction (black line), C21-C31 direction (red line), C2-CoM of lipid tails (green line), and direction normal to the instantaneous plane of the lipid tails (blue line).

components to the instantaneous plane of the lipid. This plane is defined by the vectors

$$\vec{T}_1(t) \equiv \vec{r}_{tail1\,CoM}(t) - \vec{r}_{C2}(t),$$
$$\vec{T}_2(t) \equiv \vec{r}_{tail2\,CoM}(t) - \vec{r}_{C2}(t), \tag{9}$$

where $\vec{r}_{tail1(2)\,CoM}(t)$ is the instantaneous position of the center of mass of tail 1 (2) of a lipid and $\vec{r}_{C2}(t)$ is the position of carbon C2. The perpendicular direction is defined by $\vec{N} \equiv \vec{T}_1 \times \vec{T}_2$. The results for the VACF of the velocity of the center of mass of lipid tails, as well as of its in-plane and normal components are shown in the top plot of Fig. 14. As it can be directly observed from the non-normalized VACF, the largest contribution is that of the in-plane component. The spectral densities of formed VACF are reported in the bottom plot of Fig. 14. We note that a 30 cm^{-1} peak appears in all three spectra, being a new feature not observed in the previous spectral densities of Figs. 12 and 13. Directly from our analysis, we believe that this is a clear indication that tail-groups perform "wagging" motions of low frequency, composed by motions along the in-plane direction, with some smaller component along the normal direction.

We have also analyzed the orientation and reorientation dynamics of some relevant directions of the lipid, namely (a) P-N, (b) C21-C31, (c) C2-CoM of lipid tails, and (d) the normal direction to the instantaneous plane formed by lipid tails. In Fig. 15 we show the angular distribution for each direction with the bilayer normal direction (Z). Additionally, following previous works,[14,73–77] we computed the reorientational correlation functions

$$C_2(t) = \langle P_2[\hat{u}(0) \cdot \hat{u}(t)] \rangle, \tag{10}$$

where $P_2(x)$ is the second Legendre polynomial and $\hat{u}(t)$ is the unit vector along the selected directions. We considered a double exponential to fit the decay of $C_2(t)$, with characteristic times τ_1 and τ_2. The results for the reorientational times are summarized in Table IV. We observe that the decay of the P-N vector is the fastest. The direction C21-C31 (roughly normal to the C2-tails' CoM) is the second fastest, whereas the two remaining vectors show the slowest decay times. These results are in good agreement with those obtained by Patra *et al.*[75]

A detailed inspection of such angular distributions can be performed considering angular variations of each selected direction with respect to its initial orientation at a given time (regardless of its orientation from the bilayer normal), considering time intervals of lengths τ_1 and τ_2. We obtained that at the scale of τ_1 (short reorientational times), the angle formed by each vector fluctuates around low values (around 15°–20° related to its initial orientation), whereas at the τ_2 time scale (long reorientational times), the distribution of angular variations spreads out significantly, with maxima up to 40° for the P-N direction, covering almost the full angular range. In summary, at the scale τ_1 unit vectors fluctuate narrowly and when they reach the τ_2 time scale, their orientations fluctuate to a wide range of values.

TABLE IV. Reorientational times of selected vectors in lipids (in ns).

Vector	τ_1	τ_2
P-N	0.3	2.4
C2-CoM$_{\text{tails}}$	1.5	8.3
C21-C31	0.8	6.4
Normal to tails' instantaneous plane	1.1	6.0

IV. CONCLUDING REMARKS

A series of molecular dynamics simulations of a fully hydrated DMPC lipid bilayer membrane in its liquid phase has been performed using the recently parameterized CHARMM36 force field. The system is described in atomic detail and molecules are held together with flexible bonds.

Using this description, a surface area per lipid of 60.5 Å^2 is obtained after a 30 ns equilibration in the NPT ensemble, in good agreement with the experimental value of 60.6 Å^2. From the pressure profile along the lipid bilayer we obtain the surface tension of the membrane to be of -0.1 ± 1.2 mN/m, close to the expected value of zero. Other structural properties obtained from our description, such as the density profiles or the deuterium order parameter, are in good agreement with experimental and simulation works.

Diffusion of lipids in the membrane and of its hydration water has also been considered. Three regions were defined for water: "bulk" water (more than 6 Å away from the position of any lipid site), "intermediate" water (between 3 and 6 Å of any lipid sites), and "contact" water (within 3 Å of any lipid sites). We found that water molecules located close to lipid sites diffuse about one order of magnitude slower than those at intermediate and bulk-like regions. Lipid lateral diffusion is one of the most challenging properties to obtain, since it requires long simulation runs, of the order of hundreds of nanoseconds. In the present work, we studied diffusion at different time scales, from the sub-picosecond time scale (ballistic motions) to the scale of hundred nanoseconds (Fickian diffusion). In between, we found a sub-diffusive regime (range between 0.01 and 10 ns), where the lipid diffusion coefficient is about (2–9) $\times$ 10^{-7} cm^2/s. In this regime, particles at the lipid head-group move significantly faster than those located at the body center and slower than those at tail-groups. In the longest time scale analyzed in the present work, lateral diffusion of lipid chains is essentially Fickian, as the result of a global motion of each lipid chain. In this regime we obtained a diffusion coefficient of 0.61 $\times$ 10^{-7} cm^2/s, very close to the experimental result obtained from FRAP experiments of 0.59 $\times$ 10^{-7} cm^2/s.[55] Regarding the mechanism of lipid diffusion at long timescales, we have identified the existence of nanodomains in which the dynamics of lipids is strongly correlated, creating concerted local lipid flow in particular directions, in overall agreement with previous works.[9,10] The typical length of displacement of a nanodomain can be of 2 nm after 100 ns; they are formed by less than 10 lipid units.

We have also performed a thorough analysis of the spectroscopic properties of the lipid membrane and its hydration water by calculating the spectral densities of the corresponding atomic velocity autocorrelation functions. Our analysis gives some clues to interpret the location of frequency maxima experimentally observed in these systems using different spectroscopic techniques. Overall, our results for lipid atoms are in good agreement with available experimental data[67–70,72] measured by means of FTIR spectroscopy, mostly concerning vibrational modes of CH_2 and CH_3 units, as well as a variety of motions mediated by oxygen, phosphorus, and nitrogen. From our analysis we also obtain vibrational modes related to N-P vibrations and located around 500 cm^{-1}. The spectroscopic properties of hydration water are also well accounted for by our simulations, reproducing the three vibrational bands observed in experiment.[64,66] We also obtain the spectral band related to the motion of the center of mass of water at low frequencies, in agreement with far infrared and Raman spectroscopy measurements.[59,60] The effect of the interaction with the lipids on the spectroscopic properties of hydration water is also studied, resulting in the blue-shift of certain bands for water molecules in contact with the lipid membrane.

A detailed analysis of lipid reorientations and slow motions has revealed the existence of a low frequency band around 30 cm^{-1} that can be assigned to wagging of the tail vibrations which are motions of the tail-groups along the instantaneous plane formed by the two tails of each lipid. In addition, we have analyzed the reorientation dynamics of lipid tails, which can be characterized by two time-scales.

ACKNOWLEDGMENTS

J.M. gratefully acknowledges financial support from the *Direcció General de Recerca de la Generalitat de Catalunya* (Grant No. 2009-SGR-1003) and the Spanish MICINN for Grant No. FIS2012-394-C02-01. C.C. thanks the financial support from the Technical University of Catalonia for a postdoctoral fellowship. J.Y. is a recipient of an AGAUR-FI Catalan fellowship.

[1] J. F. Nagle and S. Tristam-Nagle, Biochim. Biophys. Acta **1469**, 159 (2000).
[2] S. Schürch, M. Lee, and P. Gehr, Pure Appl. Chem. **64**, 1745 (1992).
[3] S.-J. Marrink and H. J. C. Berendsen, J. Phys. Chem. **98**, 4155 (1994).
[4] S. Y. Bhide and M. L. Berkowitz, J. Chem. Phys. **123**, 224702 (2005).
[5] L. Rosso and I. R. Gould, J. Comput. Chem. **29**, 24 (2008).
[6] W. Zhao, D. E. Moilanen, E. E. Fenn, and M. D. Fayer, J. Am. Chem. Soc. **130**, 13927 (2008).
[7] C. L. Armstrong, M. Trapp, J. Peters, T. Seydel, and M. C. Rheinstädter, Soft Matter **7**, 8358 (2011).
[8] S. König, W. Pfeiffer, T. Bayerl, D. Richter, and E. Sackmann, J. Phys. II **2**, 1589 (1992).
[9] E. Falck, T. Róg, M. Karttunen, and I. Vattulainen, J. Am. Chem. Soc. **130**, 44 (2008).
[10] S. Busch, L. C. Pardo, C. Smuda, and T. Unruh, Soft Matter **8**, 3576 (2012).
[11] C. L. Armstrong, M. D. Kaye, M. Zamponi, E. Mamontov, M. Tyagi, T. Jenkins, and M. C. Rheinstädter, Soft Matter **6**, 5864 (2010).
[12] A. A. Gurtovenko and I. Vattulainen, J. Phys. Chem. B **111**, 13554 (2007).
[13] J. Martí and F. S. Csajka, Phys. Rev. E **69**, 061918 (2004).
[14] J. Wohlert and O. Edholm, J. Chem. Phys. **125**, 204703 (2006).
[15] M. Kozak, A. Wypych, K. Szpotkowski, S. Jurga, and A. Skrzypczak, J. Non-Cryst. Solids **356**, 747 (2010).
[16] E. Flenner, J. Das, M. C. Rheinstädter, and I. Kosztin, Phys. Rev. E **79**, 011907 (2009).
[17] F. Y. Hansen, G. H. Peters, H. Taub, and A. Miskowiec, J. Chem. Phys. **137**, 204910 (2012).
[18] J. B. Klauda, R. M. Venable, J. A. Freites, J. W. O'Connor, D. J. Tobias, C. Mondragon-Ramirez, I. Vorobyov, A. D. MacKerell, Jr., and R. W. Pastor, J. Phys. Chem. B **114**, 7830 (2010).
[19] W. L. Jorgensen, J. Chandrasekhar, J. D. Madura, R. W. Impey, and M. L. Klein, J. Chem. Phys. **79**, 926 (1983).
[20] M. Praprotnik and D. Janežič, J. Chem. Phys. **122**, 174103 (2005).
[21] J. F. Nagle, R. Zhang, S. Tristam-Nagle, H. I. Petrache, and R. M. Suter, Biophys. J. **70**, 1419 (1996).
[22] J. C. Phillips, R. Braun, W. Wang, J. Gumbart, E. Tajkhorshid, E. Villa, C. Chipot, R. D. Skeel, L. Kale, and K. Schulten, J. Comput. Chem. **26**, 1781 (2005).

[23]U. Essmann, L. Perera, M. L. Berkowitz, T. Darden, H. Lee, and L. G. Pedersen, J. Chem. Phys. **103**, 8577 (1995).
[24]P. R. Pandey and S. Roy, J. Phys. Chem. B **115**, 3155 (2011).
[25]J. B. Klauda, N. Kučerka, B. R. Brooks, R. W. Pastor, and J. F. Nagle, Biophys. J. **90**, 2796 (2006).
[26]H. J. C. Berendsen, J. P. M. Postma, W. F. van Gunsteren, A. DiNola, and J. R. Haak, J. Phys. Chem. **81**, 3684 (1984).
[27]S. E. Feller, Y. Zhang, R. W. Pastor, and B. R. Brooks, J. Chem. Phys. **103**, 4613 (1995).
[28]E. Lindahl and O. Edholm, J. Chem. Phys. **115**, 4938 (2001).
[29]G. W. Stockton and I. C. P. Smith, Chem. Phys. Lipids **17**, 251 (1976).
[30]C. Hofsäss, E. Lindahl, and O. Edholm, Biophys. J. **84**, 2192 (2003).
[31]T. P. Trouard, A. A. Nevzorov, T. M. Alam, C. Job, J. Zajicek, and M. F. Brown, J. Chem. Phys. **110**, 8802 (1999).
[32]H. I. Petrache, S. W. Dodd, and M. F. Brown, Biophys. J. **79**, 3172 (2000).
[33]P. B. Moore, C. F. Lopez, and M. L. Klein, Biophys. J. **81**, 2484 (2001).
[34]B. Griepernau and R. A. Böckmann, Biophys. J. **95**, 5766 (2008).
[35]J. Gullingsrud, A. Babakhani, and J. A. McCammon, Mol. Simul. **32**(10–11), 831 (2006).
[36]J. Gullingsrud and K. Schulten, Biophys. J. **86**, 3496 (2004).
[37]K. Tu, D. J. Tobias, K. Basie, and M. L. Klein, Biophys. J. **70**, 595 (1996).
[38]F. Jähnig, Biophys. J. **71**, 1348 (1996).
[39]F. Brochard, P. G. de Gennes, and P. Pfeuty, J. Phys. **37**, 1099 (1976).
[40]H. Schindler, FEBS Lett. **122**, 77 (1980).
[41]D. J. Tieleman and H. J. C. Berendsen, J. Chem. Phys. **105**, 4871 (1996).
[42]E. A. Disalvo, F. Lairion, F. Martini, E. Tymczyszyn, M. Frías, H. Almaleck, and G. J. Gordillo, Biochim. Biophys. Acta **1778**, 2655 (2008).
[43]R. Hausik and S. Han, Phys. Chem. Chem. Phys. **13**, 7732 (2011).
[44]N. A. Krylov, V. M. Pentkovsky, and R. G. Efremov, ACS Nano **7**(10), 9428 (2013).
[45]K. Krynicki, C. D. Green, and D. W. Sawyer, Faraday Discuss. Chem. Soc. **66**, 199 (1978).
[46]A.-L. Kuo and C. G. Wade, Biochemistry **18**, 2300 (1979).
[47]T. Fujiwara, K. Ritchie, H. Murakoshi, and A. Kusumi, J. Cell Biol. **157**, 1071 (2002).
[48]P. F. F. Almeida and W. L. C. Vaz, *Handbook of Biological Physics* (Elsevier Science, New York, 1995).
[49]P. Schwille, J. Korlach, and W. W. Webb, Cytometry **36**, 176 (1999).
[50]J. Tabony and B. Perly, Biochim. Biophys. Acta **1063**, 67 (1991).
[51]G. Palermo, P. Campomanes, M. Neri, D. Piomelli, A. Cavalli, U. Rothlisberger, and M. De Vivo, J. Chem. Theory Comput. **9**, 1202 (2013).
[52]J.-H. Jeon, H. M.-S. Monne, M. Javanainen, and R. Metzler, Phys. Rev. Lett. **109**, 188103 (2012).
[53]E. Barkai, Y. Garini, and R. Metzler, Phys. Today **65**, 29 (2012).
[54]I. M. Sokolov, Soft Matter **8**, 9043 (2012).
[55]W. L. C. Vaz, R. M. Clegg, and D. Hallmann, Biochemistry **24**, 781 (1985).
[56]S. Feller and J. MacKerell, J. Phys. Chem. B **104**, 7510 (2000).
[57]D. A. McQuarrie, *Statistical Mechanics* (Harper and Row, New York, 1976).
[58]J. Martí, E. Guàrdia, and J. A. Padró, J. Chem. Phys. **101**, 10883 (1994).
[59]G. E. Walrafen, M. R. Fischer, M. S. Hokmabadi, and W. H. Yang, J. Chem. Phys. **85**, 6970 (1986).
[60]I. Ohmine and H. Tanaka, Chem. Rev. **93**, 2545 (1993).
[61]A. Debnath, B. Mukherjee, K. G. Ayappa, P. K. Maiti, and S.-T. Lin, J. Chem. Phys. **133**, 174704 (2010).
[62]B. Hasted, S. K. Husain, F. A. M. Frescura, and J. R. Birch, Chem. Phys. Lett. **118**, 622 (1985).
[63]J. A. Padró and J. Martí, J. Chem. Phys. **120**, 1659 (2004).
[64]E. A. Disalvo and M. A. Frias, Langmuir **29**, 6969 (2013).
[65]D. Eisenberg and K. Kauzmann, *The Structure and Properties of Water* (Clarendon, Oxford, 1969).
[66]M. Moskovits and K. H. Michaelian, J. Chem. Phys. **69**, 2306 (1978).
[67]W. Pohle, D. R. Gauger, H. Fritzsche, B. Rattay, C. Selle, H. Binder, and H. Böhlig, J. Mol. Struct. **563–564**, 463 (2001).
[68]H. Binder, Appl. Spectrosc. Rev. **38**, 15 (2003).
[69]W. Hübner and H. H. Mantsch, Biophys. J. **59**, 1261 (1991).
[70]H. Binder, T. Gutberlet, A. Anikin, and G. Klose, Biophys. J. **74**, 1908 (1998).
[71]S. Krishnamurty, M. Stefanov, T. Mineva, S. Bégu, J. M. Devoiselle, A. Goursot, R. Zhu, and D. R. Salahub, J. Phys. Chem. B **112**, 13433 (2008).
[72]D. R. Gauger and W. Pohle, J. Mol. Struct. **744–747**, 211 (2005).
[73]R. W. Pastor, R. M. Venable, and M. Karplus, J. Chem. Phys. **89**, 1128 (1988).
[74]R. W. Pastor, R. M. Venable, and S. E. Feller, Acc. Chem. Res. **35**, 438 (2002).
[75]M. Patra, M. Karttunen, M. T. Hyvönen, E. Falck, and I. Vattulainen, J. Phys. Chem. B **108**, 4485 (2004).
[76]J. B. Klauda, N. V. Eldho, K. Gawrisch, B. R. Brooks, and R. W. Pastor, J. Phys. Chem. B **112**, 5924 (2008).
[77]J. B. Klauda, M. F. Roberts, A. G. Redfield, B. R. Brooks, and R. W. Pastor, Biophys. J. **94**, 3074 (2008).